# Solar-Integrated Interleaved Direct Current Charging System for Electric Vehicles

Saumya Singh[1] and R. K. Saket[1,*]

ARTICLE INFO

*Article history:*
Received: 28 June 2024
Revised: 2 September 2024
Accepted: 21 September 2024
Online: 15 May 2026

*Keywords*:
Interleaved boost converter (IBC)
PI Controller
MPPT Technique
Electric vehicles (EVs)
Solar to Vehicle (S2V)

ABSTRACT

This research presents a new solar-integrated, interleaved direct current (DC) charging method for electric vehicles (EVs) called Maximum Power Point Tracking (MPPT). The system uses special coils in connected power-increasing devices to make them work better and last longer. This is important because it reduces energy waste and helps the environment. A key focus is integrating photovoltaic (PV) battery storage with EV battery systems, optimizing the charging process through a sophisticated MPPT algorithm. This ensures solar panels operate at their maximum power output, even under changing environmental conditions. The proposed charging system, evaluated via Simulink/MATLAB simulations, demonstrates superior performance with a notable energy efficiency of 96.8%. The results validate the efficacy of interleaved boost converter design in mitigating ripple effects and switching losses, thereby improving overall system reliability and efficiency. This advanced charging solution offers a significant step forward in sustainable energy applications for electric vehicles, promoting cleaner and more efficient transportation.

## 1. INTRODUCTION

The increasing interest in solar-to-vehicle (S2V) charging systems is driven by the growing adoption of EVs and the demand for sustainable energy solutions. Recently, there has been a significant increase in the focus on renewable energy sources because of the environmental issues and the escalating costs of fossil fuels. The most widely used renewable energy source nowadays is photovoltaic systems, which use solar radiation to generate electrical energy [1, 2]. A photovoltaic array's MPP able to be monitored by adjusting the duty cycle of DC-DC coverterusing MPPT techniques. MPPT algorithm identifies optimal duty cycle by comparing voltage and current of PV panel up to reference value. This reference value is generated using a specific MPPT algorithm. Consequently, designing an efficient MPPT techniques are crucial to extract maximum available power, especially in large solar PV setups. Various MPPT techniques, including the INC and methods for perturbation (P&O) have been extensively studied in the literature. One common MPPT technique is the P&O algorithm recognized for its simplicity and computational efficiency [4].

Research on EV systems goes beyond analyzing the components and driving mechanisms found in cars. Charging strategies are also vital for enhancing the sustainability of EVs in the transportation sector. A DC/DC converter which can be bidirectional or boost converter is important to energy systems. It helps control the flow of harvested energy from sources like Wind turbines or solar panels. This means the energy can be used efficiently in EVs, renewable energy systems, and industrial power supplies. The converters ensure the energy is managed well and can be integrated into different power systems to meet specific needs [5]. These converters are essential for harnessing these energy sources. In the past, SCRs were used to regulate these converters. Modern switches like MOSFETs and IGBTs can operate across various frequencies [6]. Increasing the operating frequency can reduce the size and cost of inductors and capacitors [7]. Fast battery charging is essential for electric vehicles to compete with petrol stations. This research illustrates the feasibility of powering an EV solely using solar energy. Solar photovoltaic (PV) arrays are widely recognized as most accessible forms of renewable energy to deploy, and their affordability continues to improve, making them increasingly appealing. Consequently, many EV owners now prefer PV array-based vehicle charging [8, 9]. An intermediate DC/DC converter and a bidirectional converter are required in to integrate PV array with the EV battery [10–12].

The interleaving technique, or multi-phasing, utilizes a

[1]*Department of Electrical Engineering, Indian Institute of Technology (BHU), Varanasi 221005, (U.P.) India.*
**Corresponding author:* R. K. Saket; Phone: +91-988-9848-412; Email(s): rksaket@ieee.org, rksaket.eee@iitbhu.ac.in.

parallel configuration of numerous inductors, diodes, and switches connected across a single capacitor. In addition to reducing output current and voltage ripples, this technique effectively minimizes the dimensions of the filter parts. Interleaving techniques have the potential to reduce losses by means of 180-degree phase shift ripple cancellation. [13, 14]. One crucial element is the Battery Management System (BMS) in regulating the battery's stored energy to ensure dependable, effective, and secure vehicle operation. The BMS minimizes the stress on the battery when charging and discharging and avoids unanticipated current surges that might result in high discharge rates. It comprises sensors, a power delivery unit, and communication protocols [15, 16].

Additionally, the BMS is responsible for cell balancing, figuring out the state of charge (SoC), estimating the driving range, and performing various other auxiliary functions. The Energy Management System (EMS) is essential for optimizing driving range, prolonging battery life, enhancing efficiency, and ensuring electric EV's reliable operation. The SoC's principal purpose is to facilitate communication between the vehicle and the battery's inherent state, thereby preventing overcharging and excessive discharging of the battery [17]. Traveling costs are also important for EV users. Considering the travel cost for EV users is crucial to ensure that the distance between the EV and charging stations is convenient, thereby enhancing user satisfaction. A traditional interleaved boost converter (IBC) produces a voltage gain that is high. It also reduces input current ripples and improves power transfer. The interleaved quadratic high-gain chopper further enhances this [18].

The structure of this paper is outlined as follows: Section II presents the core modelling approach, including system characteristics and key design parameters. Section III details the proposed converter configuration and its control strategy for EV battery charging, along with a comparative assessment. Section IV provides the simulation results and corresponding analysis. Finally, Section V summarizes the main findings and conclusions.

## 2. MODELLING AND DESIGN

An MPPT controller's block diagram is shown in Fig.1. An MPPT controller block diagram includes several parts, including DC-DC boost converter, load or battery, controller, and PV array.

MPPT is crucial for PV charging systems, especially if solar-panel-based battery charging is involved. By maximizing the solar energy conversion process efficiency, MPPT ensures that the solar panels full output is used to charge the batteries.

In particular, when temperature and irradiance change, MPPT adjusts the battery charging current to produce faster and more efficient charging. By allowing the solar panels to absorb as much energy as possible from the sun, it optimizes the system's overall efficiency and transfers it to the battery. MPPT controllers designed for EV charging systems often integrate seamlessly with EV chargers and energy management systems. They guarantee interoperability with different EV models and charging standards by offering interfaces for tracking and managing the charging process. Maximizing renewable energy sources, an MPPT controller reduces dependency on grid electricity for EV charging. Using clean energy sources effectively can lead to cost savings and environmental benefits.

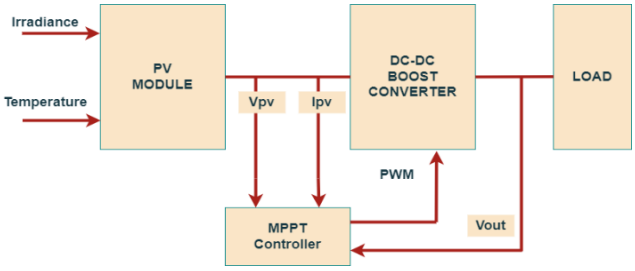


**Fig. 1. Block diagram of MPPT controller.**

### *2.1. Solar PV- Cell Model*

A photovoltaic system converts incoming solar radiation into usable electrical energy. It is becoming increasingly important in power electronics for several reasons. PV systems can be used with energy storage devices, such as batteries, to offer a reliable and consistent power source even in the absence of direct sunshine. This makes photovoltaic installations an invaluable tool for maintaining the grid's stability and resilience [19].

The circuit model's PV cell, depicted in Fig. 1, is a mathematical representation that illustrates the electrical characteristics of PV cell. This model serves as the foundation for designing and optimizing PV systems under different operating scenarios. In the equivalent circuit, the photocurrent $I_{ph}$ represents the light-generated current, the diode captures the non-linear I-V characteristics of PV cell, resistors $R_{sh}$ and Rs model the shunt and series losses, respectively.

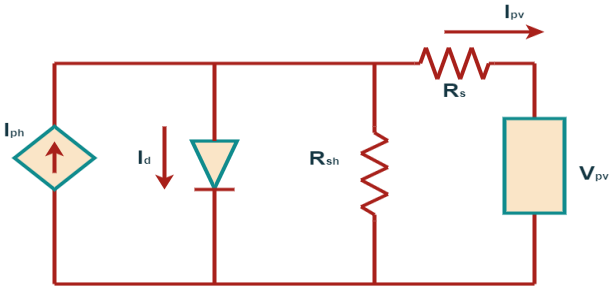


**Fig. 2. A single PV module.**

A PV cell's current-voltage curve is obtained by varying the cell's voltage and measuring the corresponding current. This curve is essential for designing PV systems as it identifies the cell's MPP, the optimal combination of voltage and current for maximizing power output. The

equation that describes current-voltage characteristics of a PV source modeled as a single diode may be shown as:

$$\boldsymbol{I_{pv} = I_{ph} - I_d\left(\frac{V_{pv}+R_s I_{pv}}{R_{sh}}\right)} \quad (1)$$

$$I_{pv}=I_{ph}- I_0\left[\exp\left(\frac{V_{pv}+R_s I_{pv}}{V_T A_d}\right)-1\right]-\left(\frac{V_{pv}+R_s I_{pv}}{R_{sh}}\right) \quad (2)$$

The parameter $I_0$ represents the reverse saturation current, while *Vpv* denotes terminal voltage of PV array. Output current of PV module (*Ipv*) follows standard 1-diode model. The thermal voltage is defined as:

$$V_T = \frac{kT}{q}$$

where, $q$ is $1.602 \times 10^{-19}\ C$, electron charge and $k$ is $1.38 \times 10^{-23}\ J/K$, Boltzmann's constant.

The photocurrent (*Iph*) is calculated using:

$$I_{ph} = \left[I_{ph_1} + K_I(T - T_0)\right]\frac{R}{R_1} \quad (3)$$

Here, $I_{ph_1}$, photocurrent at the reference temperature $T_0$, *KI*, temperature coefficient of current, and $(R/R_1)$ represents effect of incident solar irradiance on PV cell.

$$I_{ph_1} = \frac{R_{sh}+R_s}{R_{sh}} I_{sc} \quad (4)$$

The expression for reverse saturation current is:

$$I_0 = \frac{I_{sc}+K_I(T-T_0)}{\exp\left(\frac{V_{oc}+K_v(T-T_0)}{V_T A_d}\right)-1} \quad (5)$$

**Table 1. PV model parameters**

| Symbol | Parameter | Value |
|---|---|---|
| $E_G$ | energy gap | 1.11 |
| $R_s$ | series resistance | 0.23724 Ω |
| $R_{Sh}$ | parallel resistance | 224.1886 Ω |
| $V_{mp}$ | voltage (at MPP) | 30.7 *V* |
| $I_{mp}$ | current (at MPP) | 35 *A* |
| $N$ | number of series cells | 1 |
| $A_d$ | diode ideality factor | 1.019 |
| $I_{SC}$ | Short circuit current | 40 *A* |
| $V_{OC}$ | open circuit voltage | 36.3 *V* |
| $T$ | nominal temperature | $25^0$C |
| $G$ | nominal solar irradiance | 1000 $W/m^2$ |

### *2.2 PV System's Characteristics*

The photovoltaic (PV) model is developed using the parameter values listed in Table 1. To achieve a maximum power output of approximately 1000 W under test conditions, specifically solar irradiance of 1000 W/m² and cell temperature of 25°C, the system configuration consists of a single PV module connected in series with one parallel string. This arrangement ensures that model accurately reflects expected electrical behavior of PV module under ideal operating conditions.

#### *2.2.1 I–V, P–V Characteristics under different illumination levels*

Furthermore, the I–V, P–V characteristics of PV module under different illumination levels are shown in Fig. 3. These characteristics are essential for MPPT-based charging of the EV battery. Fig. 3(a) illustrates I–V curves of module at solar irradiance levels of 1 kW/m², 0.8 kW/m², 0.6 kW/m², and 0.4 kW/m². Similarly, Fig. 3(b) presents the corresponding P–V characteristics. As solar radiation decreases, short-circuit current ($I_{sc}$) reduces almost proportionally, while open-circuit voltage ($V_{oc}$) drops logarithmically. This combined reduction leads to a significant decrease in output power.

To maintain optimal operating conditions despite varying illumination, MPPT algorithms continuously adjust operating point of PV array. The controller (i) senses the instantaneous PV voltage and current, and (ii) determines operating voltage that maximizes power extraction. In I–V characteristics, $I_{sc}$ is defined as the current at zero voltage and increases linearly with irradiance due to the higher number of photon-generated carriers. Conversely, $V_{oc}$, the voltage at zero current, shows a weaker logarithmic dependence on irradiance. These behaviors underscore the importance of MPPT in ensuring PV system operates near its maximum power point under fluctuating environmental conditions.

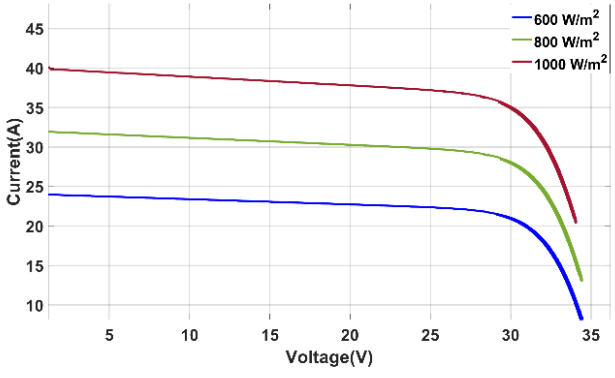


**Fig. 3. (a) Effect of Illumination Level on I–V Characteristics.**

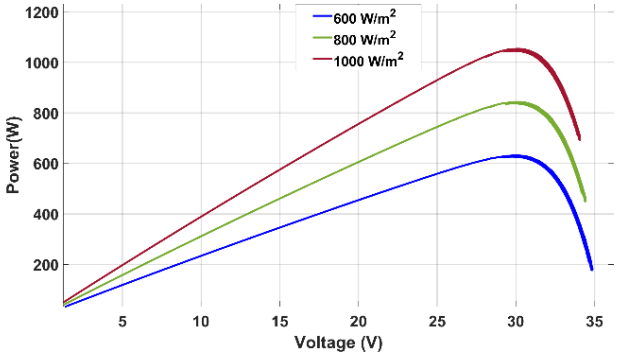


**Fig. 3 (b) Effect of Illumination Level on P–V Characteristics.**

*2.2.2 Influence of Temperature on I–V and P–V Behavior*

Fig.4 represents (a) I-V and (b) P-V characteristics of the module at different temperatures: with temperature variations, the maximum power available from the solar source varies, with $60^0$C, $45^0$C, and $25^0$C. As temperature changes, the maximum power output also varies. Therefore, an effective MPPT system should be able to tackle these changes and provide the necessary output current for battery charging. When the maximum power is high, it indicates that insolation levels are also high. Consequently, the charging current should be correspondingly high. As temperature decreased, short circuit current decreased with small values, and OC voltage increased with large values, resulting in a total increase in power, as shown in Fig.4 (a), (b). In I-V characteristics, When the temperature rises, open-circuit voltage dramatically drops while short-circuit current somewhat increases. Whenever, In P-V Characteristics, as the maximum power point changes to lower voltages, higher temperatures decrease the total power output. Short-circuit current rises with temperature. This is because higher temperatures result in increased generating more charge carriers.

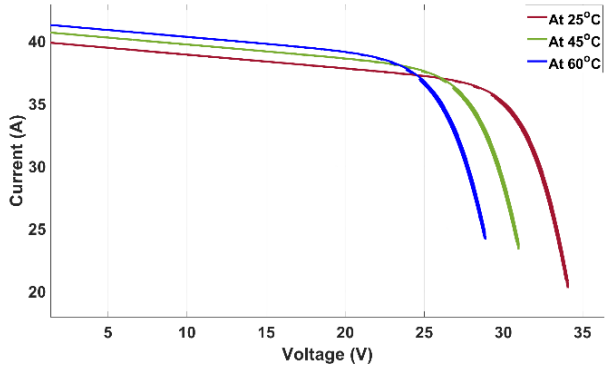


**Fig. 4. (a) I–V characteristics of PV module at different temperature levels.**

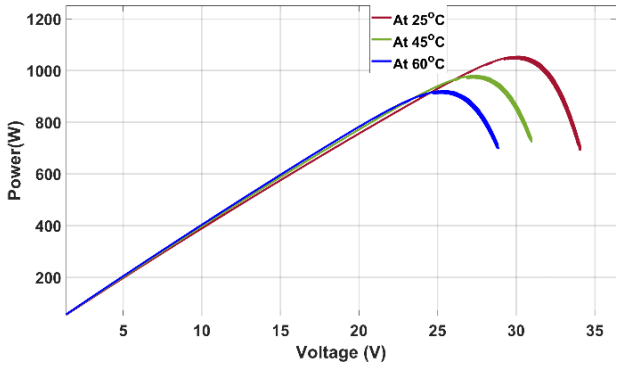


**Fig. 4. (b) P–V characteristics of PV module at different emperature levels.**

### *2.3 MPPT Controller Design*

The intersection of PV module's current–voltage curve and load line determine its natural operating point. Because this point usually deviates from, MPPT control is required to continually adjust the operating voltage and extract the highest possible power from PV system. Furthermore, load impedance can be calculated using the following method.

$$R = \frac{V_{dc}}{I} \tag{6}$$

Assume, $I_\alpha$ and $V_\alpha$ is MPP current and voltage, respectively. Then, PV optimal load can be defined as

$$R_{op} = \frac{V_\alpha}{I_\alpha} \tag{7}$$

PV systems transfer maximum power when $R = R_{op}$. MPP's location varies continuously according to irradiance and temperature, so tracking algorithms must be used to determine its location [20, 21].

### *2.4 DC-DC Boost Converter Model*

The converter model functions as a power conditioning circuit, regulating the DC supply by stepping the voltage up or down to the required level. An effective converter must exhibit low electromagnetic interference, wide bandwidth, low cost, minimal voltage and current ripple, and fast dynamic response to load or irradiation variations [22].

In MPPT-based photovoltaic systems, converter operate as a buck, boost, or buck-boost topology by adjusts PV input voltage to maintain the operating point at the maximum power point. Integrating an MPPT with the converter ensures optimal energy extraction, enhance the overall efficiency and performance of renewable energy systems. The MPPT algorithm's output controls the DC-DC converter's duty cycle, adjusting PV panel's input voltage to the optimal point. In the depicted circuit Fig. 5, the various components are designated as follows: L signifies the inductor, $Q_1$stands for the power semiconductor switch, $V_g$ indicates the supply voltage, C represents the capacitor, R signifies the load resistance, and $D_2$represents the power

semiconductor diode. Additionally, $V_{dc}$ and I denote the output voltage and current, respectively.

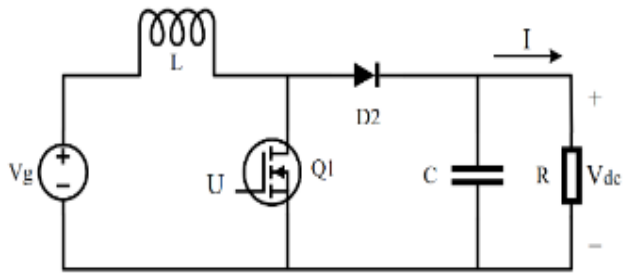


**Fig. 5. DC-DC boost converter.**

When switch is turned on, the ensuing dynamics are:

$$\begin{cases} \frac{dI_L}{dt} & = \frac{V_g}{L} \\ \frac{dV_{dc}}{dt} & = -\frac{V_{dc}}{RC} \end{cases} \quad (8)$$

When switch is turned off, the resulting dynamics

$$\begin{cases} \frac{dI_L}{dt} & = -\frac{V_{dc}}{L} + \frac{V_g}{L} \\ \frac{dV_{dc}}{dt} & = \frac{I_L}{C} - \frac{V_{dc}}{RC} \end{cases} \quad (9)$$

Based on the Figs.2 and 5, $V_{pv} = V_g$ and $I_L = I_{pv}$, then after combining (8) and (9), yields

$$\begin{cases} \frac{dI_{pv}}{dt} & = -(1-\Sigma)\frac{V_{dc}}{L} + \frac{V_{pv}}{L} \\ \frac{dV_{dc}}{dt} & = (1-\Sigma)\frac{I_{pv}}{C} - \frac{V_{dc}}{RC} \end{cases} \quad (10)$$

where Σ represents the switching position of boost converter. One can write (10) as follows:

$$\frac{dI_{pv}}{dt} = -(1-u)\frac{V_{dc}}{L} + \frac{V_{pv}}{L} \quad (11)$$

$$\frac{dV_{dc}}{dt} = (1-u)\frac{I_{pv}}{C} - \frac{V_{dc}}{RC} \quad (12)$$

where, u is the control input for the boost converter [23].

### *2.5 Interleaved Boost Converter (IBC)*

An IBC is a multi-phase DC–DC conversion topology in which several boost converter cells operate in parallel with phase-shifted switching. By distributing the current between parallel stages and shifting their gate pulses by $360^0$/n (where n, number of phases), IBC significantly reduces input/output ripple current, enhances transient response, and improves thermal performance.

In the configuration considered here, two boost stages operate in parallel with a $180^0$ phase shift at the same switching frequency. This interleaving action increases efficiency, minimizes Total harmonic distortion (THD), reduces component stress, and provides better reliability compared to a single boost converter. when the switch is opened.

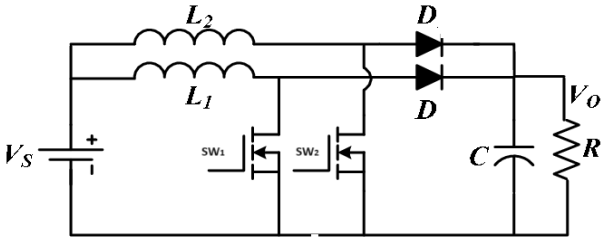


**Fig. 6. Basic circuit of IBC.**

The IBC consists of two switches ($SW_1$, $SW_2$), diodes ($D_1$, $D_2$), inductors ($L_1$, $L_2$), a storage capacitor (C), and a load resistance (R), supplied by an input source $V_s$. Each switch is controlled by a phase-shifted gating signal. Although an interleaved converter can operate in four switching modes, this study focuses on continuous conduction mode (CCM) to simplify analysis. For the presented design, the inductors are assumed identical ($L_1 = L_2 = L$), and both switches operate with the same duty cycle ($D_1 = D_2 = D$), separated by a time delay T. The operation takes place in two primary phases: during e the diode remains reverse-biased, and during switch-OFF interval, inductor releases its stored energy to the load through the forward-biased diode.

The proposed IBC configuration extends naturally to higher-phase designs (two, three, or four phases) based on the same principle of interleaving. The key electrical parameters used for sizing and simulation of the IBC are listed in the following section.

#### *2.5.1 Design Parameters Considered*

*(i) Duty Ratio*

The following is an expression for the proposed charger's duty cycle D:

$$D = 1 - \frac{V_s \times \eta}{V_o} \quad (13)$$

In a switching converter, where $V_o$ indicates the voltage output, Vs represents the input voltage, and η signifies the converter's efficiency.

*(ii) Boost Ratio*

The duty cycle governs the voltage conversion ratio in IBC, similar to conventional boost topology. It is expressed as:

$$\frac{V_o}{V_S} = \frac{1}{1-D} \quad (14)$$

where, $V_o$ is output voltage, $V_s$ is input voltage, and D denotes duty cycle.

*(iii) Input Current ( $I_{in}$)*

Current can be determined using input power and voltage.

$$I_{in} = \frac{P_{in}}{V_s} \quad (15)$$

Here, $P_{in}$ denotes i/p power, and Vs represents i/p voltage.

*(iv) Inductor-Current Ripple ($\Delta I_L$)*

When $f_s$ is switching frequency, D represents the duty cycle, $V_S$ is i/p voltage, and L denotes inductance.

Then Inductor-Current Ripple:

$$\boldsymbol{\Delta I_L = \frac{V_s \cdot D}{L \cdot f_s}} \quad (16)$$

*(v) Selection of Inductor and Capacitor*

During operation of an interleaved DC–DC boost converter, energy is first transferred from the input source to the inductor and subsequently delivered from the inductor to the output. For balanced current sharing between phases, both inductors must be identical in value and characteristics. In the proposed charger, the resonant interaction between the inductor LLL and capacitor CCC helps smooth the switch voltage during turn-off, reducing stress on the semiconductor devices. Based on this operation, the required energy stored in the passive components can be estimated, and their values are selected using the following expressions.

The inductance is given by

$$\boldsymbol{L = \frac{V_S \cdot D}{\Delta I_L \cdot f_s}} \quad (17)$$

where, Vs, the input voltage, $\Delta I_L$, inductor current ripple, D, duty ratio, and $f_s$ , switching frequency. The output capacitor value is determined by

$$\boldsymbol{C = \frac{V_o \cdot D}{\Delta V_o \cdot R \cdot f_s}} \quad (18)$$

where $R$ is the load resistance and $\Delta V_o$ the allowable output voltage ripple.

*(vi) Resistance (R)*

A developed technique for overcoming the drawbacks of conventional boost converters is called interleaving or multi-phase. The filter's components can be reduced by organizing the parts in a parallel configuration with two switches, diodes, and one coupled inductor to a single capacitor and load. The resistance or load, R, expressed as equation (19):

$$\mathbf{R} = \frac{V_{out}}{I_{out}} \quad (19)$$

### *2.6 Parameters Considered*

To create a design parameter specification table for a proposed converter, we must include various key parameters defining the converter's performance, capabilities, and constraints. This table comprehensively overviews a proposed converter's specifications and design parameters.

**Table 2. Specifications of the proposed converter**

| Parameters | Values |
|---|---|
| Source Voltage, $V_s$ | 30 V |
| Source current, $I_s$ | 35 Amp |
| Battery Voltage, $V_0$ | 48 V |
| output current, $I_o$ | 20 Amp |
| Output Power, $P_0$ | 1KW |
| Output voltage ripple, $V_0$, ripple (t) | 5% of output voltage ($V_0$) |
| Switching frequency, $f_s$ | 20kHz |
| Inductance $L_1$, $L_2$ | 9$\mu$H |
| Capacitance C | 470$\mu$F |

## 3. PROPOSED METHOD: CIRCUIT DESCRIPTION

This study investigates the application of an interleaved boost converter in a PV-powered EV charging system, as shown in Fig. 7. The converter is governed by a PI-based control scheme that manages the switching operation during battery charging and discharging. This control strategy ensures stable voltage regulation and smooth operation of the converter.

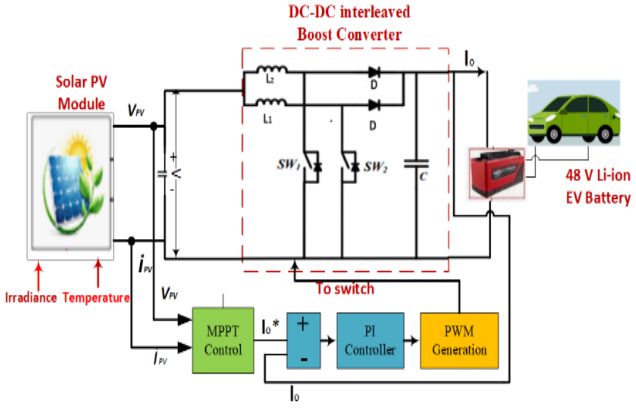


**Fig. 7. Configuration of interleaved boost converter PV-fed EV System.**

To maximize the energy harvested from the solar PV array under varying irradiation levels, an MPPT algorithm is integrated into the system. MPPT controller continuously adjusts operating point of PV module, ensuring uninterrupted EV charging even during fluctuating environmental conditions.

Closed-loop control framework is implemented to operate the converter in boost mode, coordinating the MPPT output with the PI-controlled current and voltage loops.

High-efficiency at low voltage power MOSFET switches

are employed in it, with fast switching capability, and suitability for high-frequency operation.

### *3.1 Control Technique*

Two control strategies are incorporated in the proposed system. For the solar PV stage, MPPT algorithm is employed to ensure continuous extraction of highest available power, even under non-uniform irradiance or partial shading. When some PV modules are shaded, the remaining modules continue to supply energy, allowing the EV battery to charge reliably. Its controller dynamically adjusts PV operating point in response to the load and battery charging requirements.

The overall regulation of the converter is achieved through a closed-loop control structure composed of outer voltage loop and inner current loop, as reflected in Fig. 8. The measured battery voltage ($V_b$) is compared with the reference voltage (Vref), and the resulting error is processed by a PI controller. This controller reduces the steady-state deviation and generates the reference current for the inner loop. A second PI controller then regulates the inductor current, and its output drives the PWM modulator to control the power switches. The PI compensators are characterized by their proportional and integral gains, $K_P$ and $K_I$, respectively, which determine the dynamic response of the system.

$$\boldsymbol{G(s) = K_P + \frac{K_I}{s}} \quad (20)$$

This is then fed back to the current loop iteration. Finally, the difference, when compared to the battery current ($I_b$), is sent to the PWM modulator via another PI controller. This controller helps achieve a stable PV voltage and EV battery current. When switch $SW_1$ is activated, the current in inductor $L_1$ begins to increase linearly, storing energy in the inductor during this phase. When SW1 turns OFF, diode D1 conducts and L1 discharges its stored energy based on input–output voltage difference. Inductor then discharges, delivering current to the load through diode. After half of SW1's switching cycle, SW2 begins its operation., $SW_2$ is activated, repeating the same sequence of operations. By merging the two power paths at the output capacitor, the ripple frequency doubles compared to a single-phase boost converter, resulting in significantly lower input current ripple. Here, *Vo* is the output voltage, *Vin* is the input voltage, and *D* denotes the duty cycle.

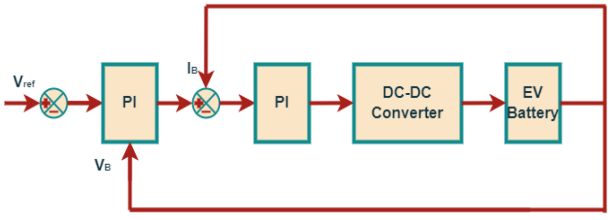


**Fig. 8. DC-DC converter closed-loop control circuit.**

The performance of the conventional boost converter and IBC with two, three, and four phases has been analyzed in [21, 25], and the comparative results are presented in Table. 3 below

**Table 3. Performance Comparison of the Boost Converter (BC) and Interleaved Boost Converter (IBC)**

| Parameters | BC [21] | BC [25] | Proposed converter (IBC) |
|---|---|---|---|
| O/P Voltage (*Vo*) | 29.25 V | - | 48 V |
| O/P Voltage ripple (%) | 0.46 | 3 % peak to peak | 0.2 |
| O/P current ripple (%) | 0.19 | 5 % peak to peak | 0.01 |
| I/P Current ripple (%) | 0.15 | - | 0.05 |
| Efficiency (%) | 95.4 | 90-92% | 96.8 |
| Voltage stress | - | High | high |
| Current stress | high | low | low |

The approach used for comparing the power quality produced by the two converters focuses on reducing O/P current and voltage ripple effects through interleaving techniques. This, in turn, decreases switching losses and enhances efficiency. In practice, the traditional boost converter's fixed gain is limited because achieving a high output voltage requires a high duty ratio, meaning the switch remains ON for extended periods. A high current in the diode can cause the reverse recovery phenomenon. Mathematical analysis and simulation results comparing the traditional boost converter and the IBC demonstrate that the IBC reduces current and voltage ripple and decreases voltage stress across the switch, as shown in Fig. 9. As a result, the IBC shows improved efficiency compared to the traditional boost converter as shown in Table 3. Finally, the analysis and simulation results are encouraging, indicating that practical implementation of the IBC would be advantageous in future work.

## 4. SIMULATION RESULTS AND DISCUSSION

This section evaluated the interleaved DC-DC boost converter model's performance using MATLAB Simulink software. In the first step, varying irradiances are used to examine MPPT's effectiveness, and later, varying temperatures are used to examine MPPT's effectiveness. The figures below represent different parameters, such as the battery's SoC at varying PV side irradiation levels, PV module, solar voltage, current and associated power, inductor current, battery current, and voltage stress on switches. The findings demonstrate that, in comparison to low radiation and high temperature settings, photovoltaic

cells perform more effectively in high radiation and low temperature environments. Therefore, to maximize the amount of incoming solar radiation, or W/m², PV cells should be kept clean and fitted with a solar tracking system for optimal performance [27].

To assess the effectiveness of the proposed topology, the final testing incorporates the following converter parameters: inductance is L = 9 μH, capacitance is C = 470 μF, and switching frequency is $f_s$ = 20kHz. The battery specifications used for evaluation include a capacity of 10 Ah, an initial state of charge of 60%, and a nominal voltage of 48 V. Fig. 9 shows that PV module delivers a maximum power of approximately 1050 W at an irradiance level of 1000 W/m².

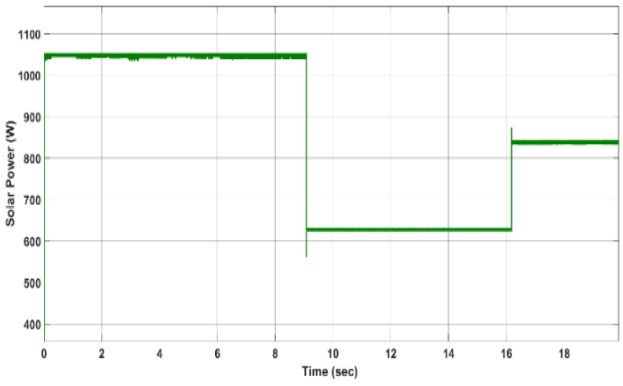


**Fig. 9. Solar power.**

Fig. 10 presents the voltage (red) and current (blue) characteristics of PV module at 1000 W/m² and 25°C, highlighting their variation in response to changes in irradiance.

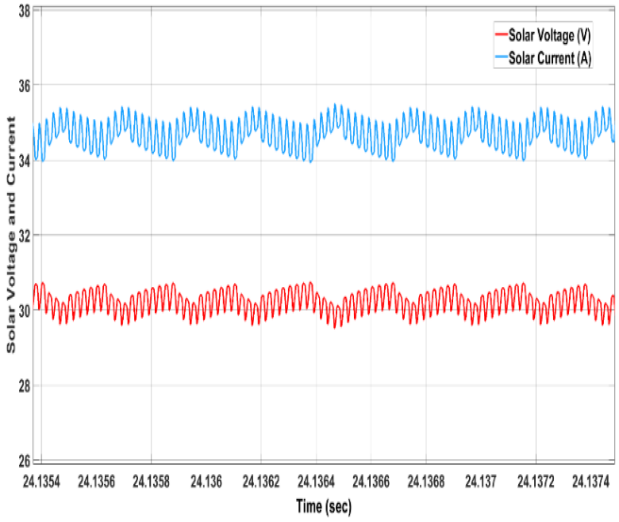


**Fig. 10. Solar voltage current**

Fig.11 illustrates the charging process with a corresponding negative battery current. In Fig.12, the voltage stress in discontinuous conduction mode (DCM) is indicated in red for switch $S_1$ and blue for switch $S_2$. Fig.13 depicts the inductor current, with the current flowing through inductor $L_1$ in green and the current through inductor $L_2$ in blue. In Fig.14, the voltage increases gradually, indicating that the EV battery is in charging mode. After transferring output voltage of PV module, optimized by the MPPT technique, to the battery side using an interleaved boost converter, Fig.14 illustrates corresponding battery charging voltage and battery's state of charge. The Fig.14 also depicts a voltage rising trend, indicating that the EV battery is in charging.

To assess the performance of the proposed topology, the final testing will involve applying various load conditions, such as a 72-volt battery, and using the different parameter values. After incorporating a 72-volt battery on the load side during the simulation, the observed gradual increase in voltage indicates that the EV battery is actively charging. Fig.15 shows the corresponding battery charging voltage and the battery's State of Charge. This confirms the proposed methodology is effective under various conditions.

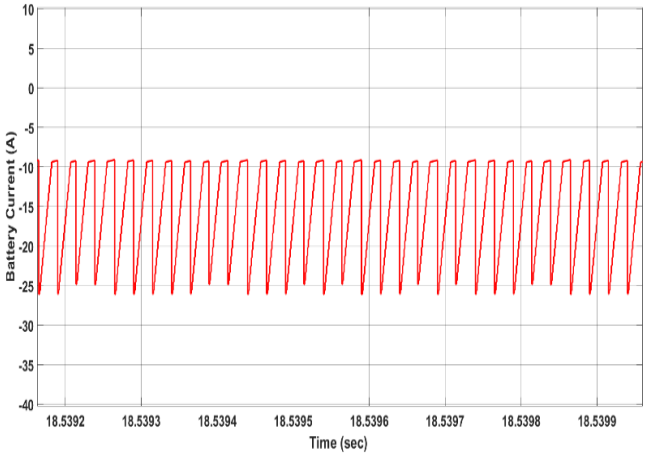


**Fig. 11. Battery currents**

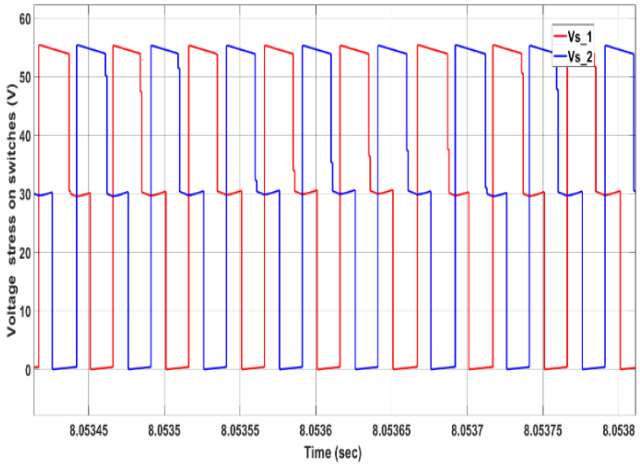


**Fig. 12. Voltage stress on switches.**

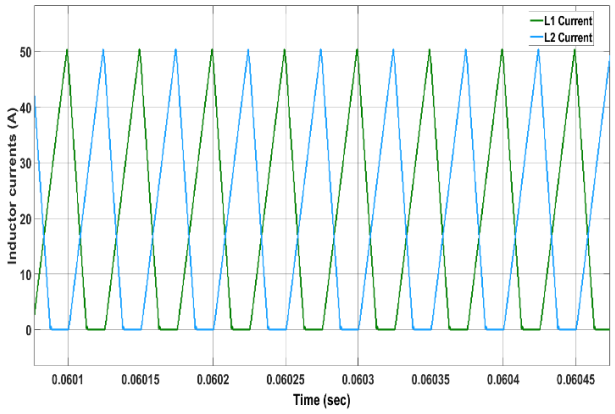


**Fig. 13. Inductor currents.**

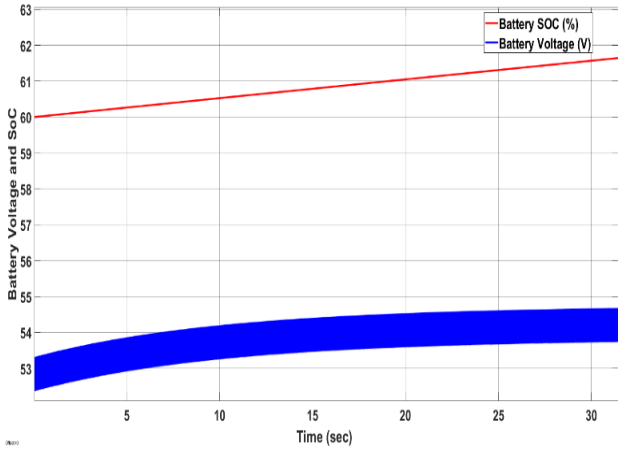


**Fig. 14. SoC and voltage profile of the 42-V battery.**

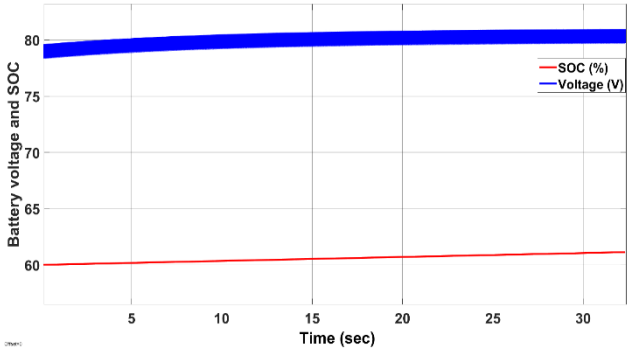


**Fig. 15. SoC and voltage profile of the 72-V battery.**

## 5. CONCLUSION

Electric Solar cars with hybrid technology have recently gained popularity due to their integration of solar PV panels. The interleaved boost converter has demonstrated greater potential than standard boost converter in reducing current and voltage ripple and improving efficiency. This paper explores an optimal charging method for a PV system utilizing the MPPT technique and an EV battery system. Reducing ripple in the IBC directly decreases switching stress, resulting in improved power-conversion efficiency. The number of inductors and capacitors used in these topologies is significantly lower.

The operation of this converter is regulated by a PI controller, enabling switching between charging and discharging modes. Furthermore, an MPPT scheme is integrated to optimize PV power output as solar irradiance fluctuates. The proposed charging system, evaluated using Simulink/MATLAB simulations, shows excellent performance with a remarkable energy efficiency of 96.8%. These results demonstrate that the interleaved boost converter architecture effectively suppresses ripple and minimizes losses in switch, leading to improved system efficiency and reliability. In these proposed topologies, the reduced size of the inductor is utilized, resulting in cost-effectiveness and decreased power losses.

## NOMENCLATURE

| Symbol | Description |
|---|---|
| EVs | Electric vehicles |
| MPPT | Maximum Power Point Tracking |
| PV | Photovoltaic |
| S2V | Solar-to-Vehicle |
| INC | Incremental-Conductance |
| MPP | Maximum Power Point |
| P&O | Perturb and Observe |
| BMS | Battery Management System |
| SoC | State of Charge |
| EMS | Energy Management System |
| IBC | Interleaved Boost Converter |
| THD | Total Harmonic Distortion |
| CCM | Continuous Conduction Mode |
| DCM | Discontinuous Conduction Mode |
| $I_{ph}$ | PV cell-generated current |
| $I_0$ | Cell reverses saturation current |
| Q1 | Power semiconductor switch |
| $V_g$ | Supply voltage |
| R | Load resistance |
| D2 | Power semiconductor diode |
| $V_{dc}$, I | Output voltage, output current |
| $\boldsymbol{\Sigma}$ | Switching position of the boost converter |
| u | Control input for the boost converter |
| D | Duty cycle |
| $\eta$ | Converter efficiency |
| $V_s$ | Input voltage |
| ($P_{in}$ | Input power |

| | |
|---|---|
| L | Inductance |
| $\Delta I_L$ | Inductor current ripple |
| $K_P$ and $K_I$ | Proportional and integral gains |
| $I_b$ | Battery current |

## ACKNOWLEDGEMENTS

The authors are thankful to the Department of Electrical Engineering, Indian Institute of Technology (BHU), Varanasi (Uttar Pradesh) India for providing research facilities to complete this manuscript work.

## REFERENCES

[1] N. Rathore, N. L. Panwar, F. Yettou, and A. Gama, "A comprehensive review of different types of solar photovoltaic cells and their applications," International Journal of Ambient Energy, vol. 42, no. 10, pp. 1200–1217, 2021.

[2] K.A. Singh, A. Prajapati, and K. Chaudhary, "High-gain compact interleaved boost converter with reduced voltage stress for PV application," IEEE Journal of Emerging and Selected Topics in Power Electronics, vol. 10, no. 4, pp. 4763–4770, 2021.

[3] M. Sarvi and A. Azadian, "A comprehensive review and classified comparison of MPPT algorithms in PV systems," Energy Systems, vol. 13, no. 2, pp. 281–320, 2022.

[4] M. Kamran, M. Mudassar, M. R. Fazal, M. U. Asghar, M. Bilal, and R. Asghar, "Implementation of improved perturb & observe MPPT technique with confined search space for standalone photovoltaic system," Journal of King Saud University-Engineering Sciences, vol. 32, no. 7, pp. 432–441, 2020.

[5] V. Singh, L. Kaur, J. Kumar, and A. Singh, "Solar PV-tied electric vehicle charging system using bidirectional dc-dc converter," in 2022 Second International Conference on Power, Control and Computing Technologies (ICPC2T). IEEE, 2022, pp. 1–5.

[6] M. Unlu, S. Camur, E. Beser, and B. Arifolu, "A current-forced line-commutated inverter for single-phase grid-connected photovoltaic generation systems," Advances in Electrical and Computer Engineering, vol. 15, no. 2, pp. 85–92, 2015

[7] P. Nandi and R. Adda, "Integration of boost-type active power decoupling topology with single-phase switched boost inverter," IEEE Transactions on Power Electronics, vol. 35, no. 11, pp. 11 965–11 975, 2020.

[8] Paul, Ankita, and Krithiga Subramanian. "PV-based off-board electric vehicle battery charger using BIDC" Turkish Journal of Electrical Engineering and Computer Sciences 27.4 (2019): 2850-2865.

[9] Y. Kobayashi, M. Hamanaka, K. Niimi, K. Yukita, T. Matsumura, and Y. Goto, "Power quality improvement method using EV for PV output fluctuation" in 2018 International Conference on Smart Grid (icSmartGrid). IEEE, 2018, pp. 272–275.

[10] A. Belkaid, I. Colak, K. Kayisli, and R. Bayindir, "Design and implementation of a Cuk converter controlled by a direct duty cycle inc-ppt in PV battery system", International Journal of Smart Grid-ijSmartGrid, vol. 3, no. 1, pp. 19–25, 2019.

[11] E. Can and M. Gulbahar, "PID control of hybrid dc-dc converter system in complex load with double reference time," Tehnicˇki glasnik, vol. 18, no. 1, pp. 63–72, 2024.

[12] K. Osmani, A. Haddad, T. Lemenand, B. Castanier, and M. Ramadan, "An investigation on maximum power extraction algorithms from PV systems with corresponding dc-dc converters," Energy, vol. 224, p. 120092, 2021.

[13] X. Hu, P. Ma, J. Wang, and G. Tan, "A hybrid cascaded dc-dc boost converter with ripple reduction and large conversion ratio," IEEE Journal of Emerging and Selected Topics in Power Electronics, vol. 8, no. 1, pp. 761–770, 2019.

[14] T. V. Muni, D. Priyanka, and S. Lalitha, "Fast acting MPPT algorithm for soft switching interleaved boost converter for solar photovoltaic system," Journal of Advanced Research in Dynamical & Control Systems, vol. 10, no. 09, 2018.

[15] Singh, S., Saket, R.K., & Khan, B. (2023). "A comprehensive state-of-the-art review on reliability assessment and charging methodologies of grid-integrated electric vehicles." IET Electrical Systems in Transportation, 13(1), e12073.

[16] Ram Kumar, M. S., Reddy, C. S. R., Ramakrishnan, A., Raja, K., Pushpa, S., Jose, S., & Jayakumar, M. (2022). "Review on Li-Ion Battery with Battery Management System in Electrical Vehicle." Advances in Materials Science and Engineering, 2022(1), 3379574.

[17] S. Singh, S. K. Soni, K. A. Singh, and R. K. Saket, "Sliding Mode Control for Bidirectional DC-DC Power Converter in Electric Vehicle Charger for G2V and V2G Applications," *2023 IEEE 3rd International Conference on Sustainable Energy and Future Electric Transportation (SEFET)*, Bhubaneswar, India, 2023, pp. 1-6.

[18] Chartsuk, N., & Marongiu, B. (2019), "Optimal fast charging station for Electric Vehicles (EVs) in Muang District" Nakhon Ratchasima, Thailand. GMSARN Int. J, 13, 26-35.

[19] Vardhan, Akanksha Singh S., and Rakesh Saxena. "MPPT of Solar Energy Conversion System with Modified Perturb and Observe Algorithm Using Bisection Method" GMSARN International Journal (2023) 9, 24-32.

[20] Singh, Smriti, R. K. Saket, and Baseem Khan. "A comprehensive review of reliability assessment

methodologies for grid-connected photovoltaic systems." IET Renewable Power Generation 17.7 (2023): 1859-1880.

[21] Faraj, Karrar S., and Jasim F. Hussain. "Analysis and comparison of DC-DC boost converter and interleaved DC-DC boost converter." Engineering and Technology Journal 38.5A (2020): 622-635.

[22] Nagaraju, Aaddagatla, and Rajender Boini. "Transformer Less Non-Isolated High Gain DC/DC Converters for Solar Photovoltaic System Applications." GMSARN International Journal 19 (2025) 199-219.

[23] S. K. Soni, S. Singh, K. A. Singh, X. Xiong, R. K. Saket, and A. Sachan, "Event-Triggered Control for LPV Modeling of DC-DC Boost Converter," in *IEEE Transactions on Circuits and Systems II: Express Briefs*, vol. 70, no. 6, pp. 2062-2066, June 2023.

[24] S. K. Soni, S. Singh, S. Kumar, H. S. Sahu, and R. K. Saket, "Solar-to-Vehicle Charging with Maximum Power Point Tracking using Super-Twisting Controller," *2023 IEEE International Transportation Electrification Conference (ITEC-India)*, Chennai, India, 2023, pp. 1-6.

[25] Rahmani, Fatemeh. "Electric Vehicle Charger based on DC/DC Converter Topology." (2018): 18879-18883.

[26] Nam, Nguyen Hoai, and Nguyen Duc Minh. "Control of Photovoltaic Cells System Based on Its Output Voltage Characteristic" GMSARN International Journal 16 (2022) 214-220.

[27] Joshi, Vivek Vardhan, Nishita Mishra, and Devesh Malviya. "Solar energy integration with new boost converter for electric vehicle application." 2018 8th IEEE India International Conference on Power Electronics (IICPE) IEEE, 2018.